Energy Recuperation in Fully Electric Vehicles Subject to Stability and Drivability Requirements

Energy Recuperation in Fully Electric Vehicles Subject to Stability and Drivability Requirements

Jóna Marín Ólafsdóttir*, Mathias Lidberg*, Paolo Falcone**
***Department of Applied Mechanics **Department of Signals and Systems,**
Chalmers University of Technology
SE-412 96 Gothenburg, Sweden

Sven van Iersel, Sven Jansen
TNO Technical Sciences, Integrated Vehicle Safety
Helmond, The Netherlands

Corresponding Author: Paolo Falcone
Phone: +46 31 772 1803
E-mail: paolo.falcone@chalmers.se

This paper presents a combined control and estimation framework for energy recuperation in fully electric vehicles. We consider a fully electric powertrain, with a driven front axle operating on low friction road surfaces. Our objective is to find the blending of regenerative and friction braking that maximizes the amount of recovered energy (i.e., the regenerative braking), while *(i)* delivering the total braking force requested by the driver, *(ii)* preserving the yaw stability as well as driveability of the vehicle. The proposed framework, which consists of a predictive braking control algorithm and a vehicle state and parameters estimator, is appealing because it requires minimal re-design efforts in order to cope with different powertrain layouts (e.g., individual wheel motors) and/or control objective and design and physical constraints. We present simulation results, obtained in three sets of manoeuvres, showing promising results in terms of energy recuperation, vehicle stability and driveability.

Topics/Integrated Chassis Control, Vehicle Dynamics Modelling and Simulation, Green-Car System Control

1. INTRODUCTION

In fully and hybrid electric vehicles, energy recuperation through regenerative braking is mainly limited by vehicle stability and drivability requirements. The regenerative braking should be used as long as the yaw motion remains close to a nominal behaviour to prevent both oversteering and understeering. Hence, blending friction braking and regenerative braking is clearly central in trading-off the energy recuperation and the vehicle dynamic behaviour. However, designing a brake blending control algorithm balancing such conflicting objectives is a challenging control problem. We start from a Model Predictive Control (MPC)-based approach presented in [1], [2] to the problem of blending friction and regenerative braking in order to satisfy the driver's braking request, while preserving the vehicle stability. In this paper, we extend the focus to include vehicle drivability issues. In particular, we focus on fully electric vehicles, where the regenerative braking is issued at the front axle. We consider manoeuvres where satisfying the driver's braking request only through regenerative braking would induce an unacceptable understeering behaviour, thus leading to serious drivability issues.

The contribution of this paper is to show how the MPC-based approach in [1], [2] can be straightforwardly extended in order to simultaneously accommodate stability and drivability requirements in brake blending applications. Furthermore, the signals used by the proposed MPC controller are generated by a Vehicle State Estimator, which provides among others, estimates of the road friction which is essential for the physical constraints we considered.

Figure 1 depicts the control scheme proposed in this paper, consisting of an MPC controller and a Vehicle State Estimator (VSE). The MPC controller commands friction and regenerative braking forces in order to satisfy the driver's braking request while preserving vehicle stability and drivability and maximizing the usage of regenerative braking. The vehicle stability and drivability are preserved by bounding the yaw rate tracking error.

Vehicle motion states, tyre normal forces and road friction estimates are provided by the VSE. Most of the signals that are required for the state estimator are available on Electronic Stability Control (ESC) systems-equipped vehicles, except the drive torques to the wheels. Nevertheless, the electric drive train provides

accurate measurements for the drive torques for acceleration and regenerative braking.

The paper is structured as follows. In Section 2 the prediction model used by the MPC controller is introduced. Section 3 presents the vehicle state estimation problem, while the control design is shown in Section 4. Simulation results are given and discussed in Section 5 and 6, respectively. Finally, Section 7 states the concluding remarks of the paper.

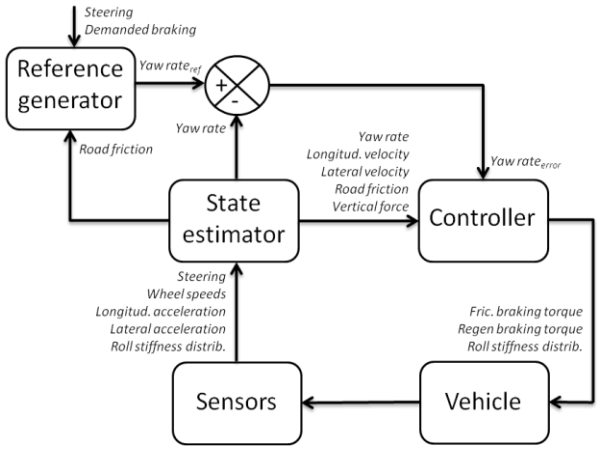

Figure 1. A scheme of the combined MPC and VSE approach to the brake blending

2. VEHICLE PREDICTION MODEL

The MPC controller utilizes a mathematical model of the vehicle to predict the future behaviour of the vehicle's states and output. The model is based on a simplified two track model depicted in Figure 2. In this paper the notations $\star$ and $\bullet$ are adopted to distinguish between variables associated with the front and rear axles of the vehicle, i.e. $\star \in f, r$, and the left and right sides, $\bullet \in l, r$. Furthermore, the subscripts *f,l; f,r; r,l; r,r* stand for front-left, front-right, rear-left and rear-right, respectively.

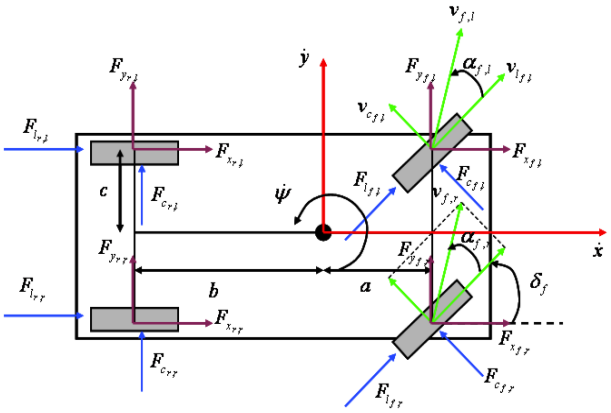

Figure 2. Schematic figure of the vehicle prediction model

The following differential equations describe the lateral, longitudinal and yaw dynamics of the vehicle:

$$m\dot{v}_y = -mv_x\dot{\psi} + F_{y_{f,l}} + F_{y_{f,r}} + F_{y_{r,l}} + F_{y_{r,r}} \quad (1)$$

$$m\dot{v}_x = mv_y\dot{\psi} + F_{x_{f,l}} + F_{x_{f,r}} + F_{x_{r,l}} + F_{x_{r,r}} \quad (2)$$

$$I\ddot{\psi} = a\left(F_{y_{f,l}} + F_{y_{f,r}}\right) - b\left(F_{y_{r,l}} + F_{y_{r,r}}\right) + c\left(-F_{x_{f,l}} + F_{x_{f,r}} - F_{x_{r,l}} + F_{x_{r,r}}\right) \quad (3)$$

where v_y is the lateral velocity, v_x is the longitudinal velocity and $\dot{\psi}$ the yaw rate. F_x and F_y are respectively the longitudinal and lateral tyre forces in the vehicle's frame of reference, m the vehicle's mass and I its inertia. The parameters a, b and c are the dimensions as depicted in Figure 2 The mapping between tyre forces in the vehicle and tyre frame is

$$F_{y_{\star,\bullet}} = F_{l_{\star,\bullet}}\sin\delta_f + F_{c_{\star,\bullet}}\cos\delta_f \quad (4)$$

$$F_{x_{\star,\bullet}} = F_{l_{\star,\bullet}}\cos\delta_f - F_{c_{\star,\bullet}}\sin\delta_f \quad (5)$$

where F_l and F_c are the longitudinal and lateral tyre forces in the tyre frame, respectively and δ is the steering angle. The longitudinal forces are assumed to be equal to the braking forces, F_b, exerted on each tyre

$$F_{l_{f,\bullet}} = F_{b_{f,\bullet}} = F_{f_{f,\bullet}} + \frac{1}{2}F_{RB} \quad (6)$$

$$F_{l_{r,\bullet}} = F_{b_{r,\bullet}} = F_{f_{r,\bullet}} \quad (7)$$

Here F_f denotes friction braking forces, i.e., forces generated by the friction braking system and F_{RB} are the forces generated by the regenerative braking system. Note that the regenerative braking forces are split equally between the front right and left wheels as the vehicle is equipped with a central drive and the front wheels are driven through a differential.

The lateral forces, F_c, are complex nonlinear functions of the road friction coefficient, tyre normal forces, slip ratios and slip angles [3]. Assuming that the vehicle operates mostly within the linear region, lateral tyre forces can be approximated as a linear function of the most governing factor, namely the slip angle α. Furthermore, when considering combined cornering and braking manoeuvres the interaction between the longitudinal and lateral forces needs to be modelled. Thus the later forces are approximated as follows

$$F_{c_{\star,\bullet}} = -C_{c_{\star,\bullet}}\alpha_{\star,\bullet} + D_{c_{\star,\bullet}}F_{l_{\star,\bullet}} \quad (8)$$

where C_c and D_c are time varying coefficients, calculated by linearizing a nonlinear tyre model, adopted from [4], around the current slip angle, longitudinal force and tyre normal load, calculated from the static load and the lateral weight transfer

$$\Delta F_{z\star} = \frac{1}{2c}\left(\frac{K_{\phi\star}}{K_{\phi t} - mh'g}h' + \frac{l - a_\star}{l}h_\star\right)ma_y \quad (9)$$

where a_y, l, h', $K_{\phi t}$ are the vehicle lateral acceleration, wheel base, centre of gravity (cog) height and roll stiffness, respectively; a and h are the distances for the axles to the cog and roll centre heights, respectively, and K_ϕ are the roll stiffnesses for the axles determined by the Roll stiffness Distribution Control (RDC) input λ

$$\begin{aligned} K_{\phi f} &= \lambda\, K_\phi \\ K_{\phi r} &= (1-\lambda)\, K_\phi \end{aligned} \tag{10}$$

By combining Equations (1) - (10) the prediction model can be written as

$$\dot{x}(t) = f(x(t), u(t), d(t)) \tag{11}$$
$$y(t) = h\big(x(t)\big) \tag{12}$$

where x denotes the state vector $x = [v_y\ v_x\ \dot{\psi}]^T$, u the input vector $u = [F_{f_{f,l}}\ F_{f_{f,r}}\ F_{f_{r,l}}\ F_{fr,r}\ F_{RB}\ \lambda]^T$, d the disturbance vector $d = [\delta_f]$ and y the output vector $y = [0\ 0\ 1]x = \dot{\psi}$.

3. VEHICLE STATE ESTIMATION

The purpose of the Vehicle State Estimator is to provide the MPC controller enhanced sensor signals, estimated vehicle signals and road friction properties. The Vehicle State Estimator used in this paper is an extension of an existing concept which is based on an Extended Kalman Filter approach [5]. The extension concerns the use of the drive torque and inclusion of rotation dynamics of the driven wheels.

The prediction model contained in the VSE is similar to the MPC model described in Section 2, but extended with rotation dynamics of the driven wheels. Such an extension accommodates road friction estimation based on wheel torque inputs, and enables the detection of μ-split conditions. The wheel dynamics are described by Equation (13) and the tyre force dependencies are provided in Equation (14)

$$I_w \dot{\omega} = T - r_{eff} F_l \tag{13}$$
$$F_l = f(\mu, F_z, \kappa, \alpha) \tag{14}$$

Here ω is the wheel rotational velocity, T is the torque acting at the wheel, I_w is the effective wheel inertia (includes part of the drive train) and r_{eff} is the effective tyre rolling radius. The longitudinal tyre force, F_l, is defined as a nonlinear function of the road friction, tyre normal force, longitudinal slip and lateral slip.

The VSE uses signals available on a modern ESC equipped vehicle. These include signals of the steering angle, longitudinal acceleration, lateral acceleration, yaw rate and wheel speeds. The estimated signals used by the MPC controller are the road friction, vertical forces, longitudinal and lateral velocity and filtered yaw rate.

4. CONTROL DESIGN

The objective of the MPC controller is to blend friction and regenerative braking in order to maximize the energy recuperated while delivering the braking force requested by the driver, fulfilling physical and design constraints and preserving the vehicle stability and drivability. In the considered vehicle layout, friction braking can be commanded at each wheel. Regenerative braking is issued at the front axle.

4.1 Cost Function

Maximizing the recuperated energy, i.e., maximizing the braking at one axle, and preserving vehicle stability and drivability are conflicting objectives that need to be balanced. We translate the conflicting objectives into the following cost function

$$\begin{aligned} &J\big(x(k), U(k), \Delta U(k)\big) = \\ &\sum_{i=0}^{H_p-1} \big\| y(k+i) - y_{ref}(k+i) \big\|_Q^2 \\ &+ \sum_{i=0}^{H_u-1} [\|u(k+i)\|_S^2 + \|\Delta u(k+i)\|_R^2] \end{aligned} \tag{15}$$

where H_p and H_u are the prediction and control horizons respectively and $U(k) = \big[u(k), \dots, u\big(k + H_p - 1\big)\big]$. Furthermore, Q and S are positive semi-definite and R a positive definite weighting matrices. Lastly, y_{ref} is the yaw rate reference, calculated based on the current steering angle, vehicle longitudinal speed and the estimated road friction coefficient [6]. The first term in the cost function penalizes deviations of the yaw rate from a reference trajectory while the second penalizes the braking forces, thus allowing the maximization of the regenerative braking force. The third and last term penalizes the rate of change of braking and contributes to smoothening of the braking commands.

4.2 System and Design Constraints

By considering the physical limitation of the braking actuators, i.e., the friction brakes and the electric motor, bounds can be set on both the braking amplitude and rates as follows

$$u_{min_{i,k}} \le u_{i,k} \le u_{max_{i,k}} \tag{16}$$
$$\Delta u_{min_{i,k}} \le \Delta u_{i,k} \le \Delta u_{max_{i,k}} \tag{17}$$
$$i = k, \dots, k + H_u - 1$$

Furthermore, since the driver's braking demand must always be fully delivered, F_D must be equal to the sum of friction and regenerative braking forces as stated by the following equalities

$$F_D = (F_{f_{f,l}} + F_{f_{f,r}} + F_{f_{r,l}} + F_{f_{r,r}} + F_{RB})_{i,k} \tag{18}$$
$$i = k, \dots, k + H_c - 1$$

where H_c is the constraint horizon.

The requested braking might exceed the tyre-road friction capabilities. This can especially occur on slippery surfaces. To prevent the controller from demanding excessive braking forces, bounds, approximating the maximum available force based on information about the road friction coefficient μ and normal tyre force $F_{z_{\star,\bullet}}$ are introduced

$$\begin{gathered}\left(F_{l_{\star,\bullet}}\right)_{i,k} \leq \left(\mu_{\star,\bullet} F_{z_{\star,\bullet}}\right)_{i,k} \\ i = k, \dots, k + H_c - 1\end{gathered} \tag{19}$$

Clearly, as long as the vehicle's energy buffer is not full it is desirable to deliver the driver's braking request through regenerative braking. Situations that may cause the regenerative braking system to be shut off by higher priority vehicle stability systems (such as, e.g., ESC or ABS) must thus be avoided. Reaching undesired yaw rate is discouraged through the first term of the cost function (15) by penalizing deviations from a reference yaw rate. However, this condition does not guarantee that the yaw rate will not deviate beyond a predefined threshold. Therefore a constraint is introduced that forces the yaw rate to stay within a certain interval. To avoid feasibility issues the constraint is relaxed (soft constrained), i.e., violations of the constraint are permitted but penalized. The constraint is formulated with respect to yaw rate error as follows

$$\begin{gathered}\dot{\psi}_{min_{i,k}} - \epsilon \leq \dot{\psi}_{i,k} - \dot{\psi}_{ref_{i,k}} \leq \dot{\psi}_{max_{i,k}} + \epsilon \\ i = k, \dots, k + H_c - 1\end{gathered} \tag{20}$$

where $\epsilon \geq 0$ is a slack variable. The cost function (15) can now be modified to include the soft constraint

$$\begin{gathered}J(x(k), U(k), \Delta U(k), \epsilon) = \\ \sum_{i=0}^{H_p-1} \left\| y(k+i) - y_{ref}(k+i) \right\|_Q^2 \\ + \sum_{i=0}^{H_u-1} \left[\|u(k+i)\|_S^2 + \|\Delta u(k+i)\|_R^2 \right] + \rho\epsilon^2\end{gathered} \tag{21}$$

4.3 State Feedback Control Law

To obtain the optimal control sequence $U_k^* = [u_{k,k}^*, \dots, u_{k+H_p-1,k}^*]$, i.e., the optimal distribution of friction and regenerative braking forces, the following open-loop optimization problem is solved

$$\begin{gathered}\min_{U_k, x_{k+1}, \dots, x_{k+H_p,k}} \quad (21) \\ subject\ to \quad (16) - (20)\end{gathered} \tag{22}$$

As problem (22) is solved in receding horizon, at time step k only the first element $u_{k,k}^*$ of the sequence U_k^* is applied to the plant while the rest of the control sequence is discarded. At the next time instant, based on the state the plant has evolved to, the optimization problem (22) is solved again over a shifted horizon.

5. SIMULATION RESULTS

The proposed approach has been tested in three challenging driving manoeuvres described next. It should be noted that in Manoeuvres 1 and 2 the RDC is excluded and the roll stiffness distribution ratio, λ, has a constant nominal value.

5.1 Manoeuvre 1: Braking in a Curve on Low-μ

In this manoeuvre the vehicle starts turning to the left, while travelling with a speed of 100 km/h on a slippery road (μ = 0.3), and increases the steering angle up to 30°. A braking command, F_D, is issued after the vehicle's yaw rate reaches a steady state value. To realize the stability performance of the vehicle in this manoeuvre without the MPC controller the vehicle's yaw rate response, when demanded braking is delivered through regenerative braking only, is plotted in Figure 3 (a).

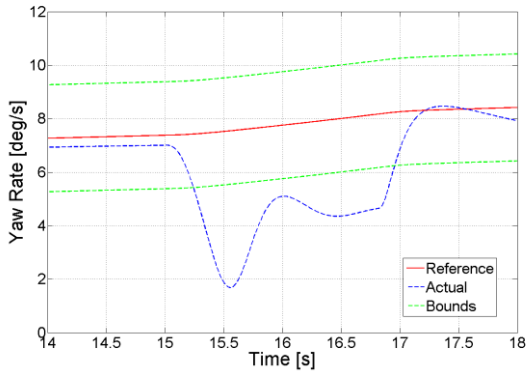

(a) Yaw rate response without the MPC controller where braking occurs at 15s

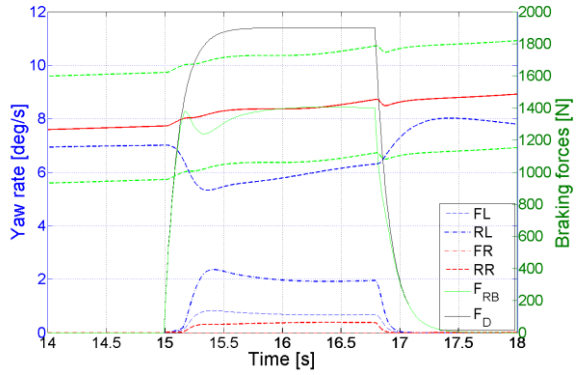

(b) Yaw rate response and braking forces with the MPC controller

Figure 3. Braking forces and yaw rate response (bold blue dashed line). Red solid line represents the yaw rate reference and green dashed lines are the upper and lower yaw rate bounds

The resulting yaw rate and braking forces issued by the controller are shown in Figure 3 (b). The figure

shows that the controller issues friction braking on three wheels in order to compensate for decreased yaw rate, induced by the regenerative braking. Note that no friction braking is issued at the front right wheel. In Manoeuvre 1 74.94% of the demanded braking is delivered through regenerative braking.

5.2 Manoeuvre 2: Straight Braking on Split-μ

In Manoeuvre 2 the vehicle is travelling straight on a slippery, split-μ surface when a braking command of 0.18g (3000N) is issued. On a split-μ surface the left and right side of the vehicle are subjected to different road friction coefficients, μ_{left} = 0.4 and μ_{right} = 0.2 respectively. In Figure 4 the braking forces are plotted w.r.t. the maximum available braking force limited by the road friction and estimated by the VSE. It shows the braking forces calculated by the controller and the bounds on braking forces defined by constraint (19). It can be observed that regenerative braking force is commanded until the force at the front right wheel reaches the bound (blue dashed line) estimated by the VSE. The achieved amount of regenerative braking is 62.23% of the demanded braking.

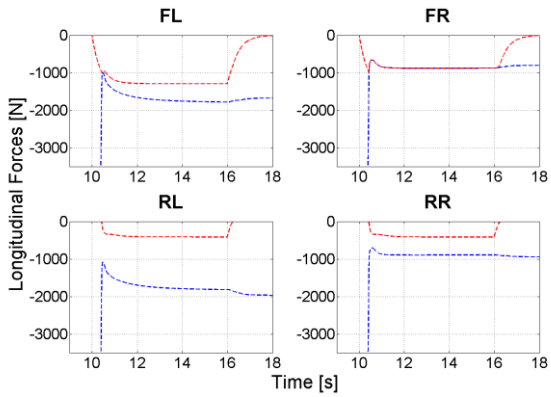

Figure 4. Commanded (red) and maximum available braking forces (bounds, blue)

5.3 Manoeuvre 3: Braking in a Curve on High-μ

In this manoeuvre the vehicle turns to the left and increases the steering angle up to 50°. The vehicle is travelling on dry asphalt (μ = 0.8) and once at steady state, a braking command of 0.2g (3400N) is issued. Manoeuvre 3 is simulated mainly to investigate the effect of including the Roll stiffness Distribution Control (RDC), see Section 2. The RDC is expected to improve the vehicle's drivability particularly in manoeuvres with high lateral accelerations. The maximum lateral acceleration in this manoeuvre is approximately 0.62 g.

Figures 5 (a) and (b) show the yaw rate responses and braking forces for two MPC controllers with fixed and varying roll stiffness distribution ratio, λ, respectively. The amount of recuperated energy is 92.52% and 94.82% of the requested braking for the controller without and with RDC, respectively.

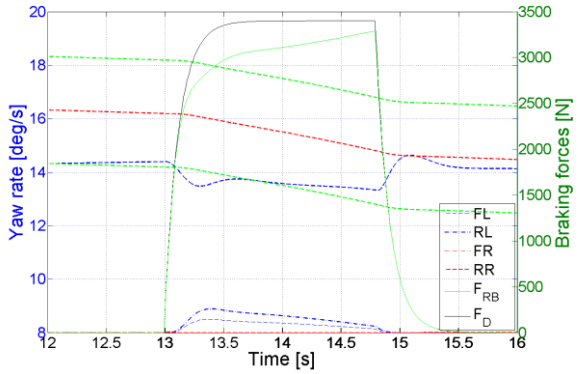

(a) Results with constant and nominal roll stiffness distribution ratio λ

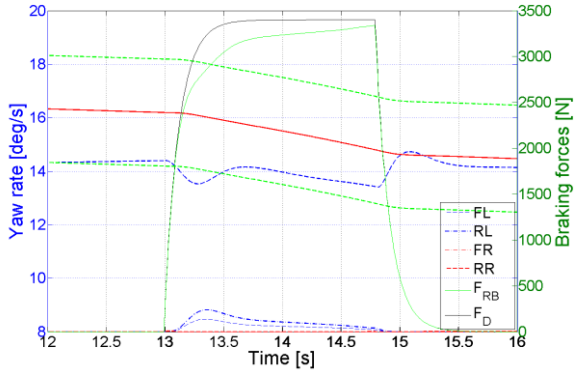

(b) Results with varying roll stiffness distribution ratio, λ, calculated by the MPC controller

Figure 5. Braking forces and yaw rate response (bold blue dashed line) without and with Roll Stiffness Distribution Control (RDC). Red solid line represents the yaw rate reference and green dashed lines are the upper and lower yaw rate bounds

5.4 VSE Performance

Figure 6 shows the estimated values for selected non-measured VSE states that are inputs to the MPC controller, compared to the actual simulated signals, for each manoeuvre. Figure 6 (a) shows that, for Manoeuvre 1, the estimated lateral velocity is a close match and even improves during braking (15 – 18s). This is due to the additional excitation of the system in this period. The left and right estimated road friction values converge well before the braking instant.

Figure 6 (b) shows the VSE performance for Manoeuvre 2. The lateral velocity for this manoeuvre is very small, and the challenge lies in the estimation of the different road friction coefficients at the left and right side of the vehicle. It is shown that these estimates converge quickly to the correct values.

In Figure 6 (c) it can be observed that for Manoeuvre 3 the estimated lateral velocity is too small, which results in too small side-slip angles at the wheels and therefore too low lateral tyre forces. This is compensated by the VSE through a slightly too high estimation of the friction coefficient. During braking the

system is again more excited and the lateral velocity and friction coefficients converge to the correct values. The VSE shows similar results with and without RDC.

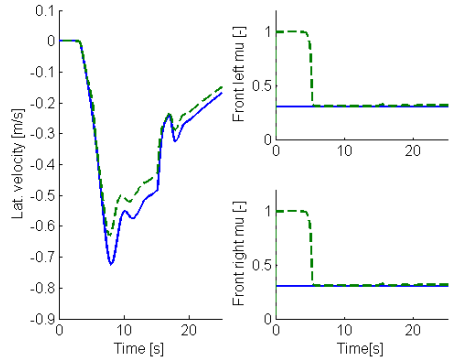

(a) Manoeuvre 1

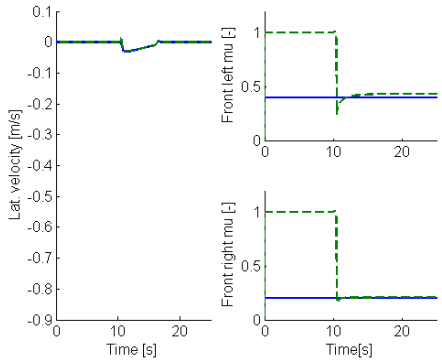

(b) Manoeuvre 2

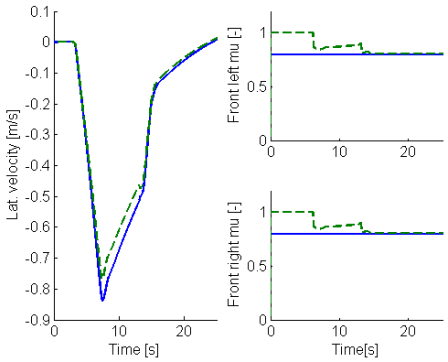

(c) Manoeuvre 3, with RDC

Figure 6. Estimated (dotted green) and simulated (solid blue) values of the vehicle lateral velocity and the left and right road friction values for the three manoeuvres

6. DISCUSSION

The control objective of maximizing the regenerative braking causes most of the braking force to be delivered at the front axle. Doing so makes the vehicle understeered and decreases the vehicle's turning rate, thus compromising the vehicle drivability. This became quite evident in Figure 3 (a) where all of the requested braking in Manoeuvre 1 was delivered through regenerative braking. The figure shows that without blending friction and regenerative braking the yaw rate bounds are severely violated during regenerative braking. In this case higher priority stability controllers might be activated and the regenerative braking simultaneously shut off.

To counteract this severe understeering effect in Manoeuvre 1, with the MPC controller, friction braking is initiated mainly on the two left wheels. By inducing braking on the left side of the vehicle understeering is decreased and violation of the yaw rate bounds is reduced.

In Manoeuvre 2, commanding braking forces that exceed the bounds on maximum allowable force calculated using the vertical wheel loads and friction estimation of the VSE, would cause the respective wheel to lock, thus compromising the stability of the vehicle. In this manoeuvre it is clear that the road friction on the right side (the low-μ side) limits the amount of achievable regenerative braking. The controller issues as much regenerative braking as constraint (19) for the front right wheel allows for, i.e., no friction braking occurs at the front right wheel. To fulfil the demanded braking request the controller delivers the remaining braking with friction braking forces equally distributed among the other three wheels.

Comparing Figures 5 (a) and (b) confirms that both yaw rate response and the amount of regenerative braking can be considerably improved with integrated RDC in a cornering manoeuvre with high lateral acceleration on a high-μ surface. The yaw rate error is greatly decreased for a controller with fixed, constant roll stiffness distribution ratio λ. Furthermore, the percentage of regenerative braking has increased by more than two percentage points.

7. CONCLUSION

We have presented a control and estimation framework for energy recuperation in fully electric vehicles. We have shown how the proposed framework can accommodate various vehicle layouts and control designs with minimal re-design efforts. Simulation results in three types of manoeuvres show that the proposed framework is capable of blending friction and regenerative braking in challenging driving scenarios where trading-off energy recuperation and vehicle stability and drivability is not trivial. The combination of the MPC controller and VSE successfully maximizes the energy recuperation w.r.t. drivability requirements, limits the vehicle understeer and fully delivers the total braking force requested by the driver.

REFERENCES

[1] P. Falcone, F. Borrelli, J. Asgari, H. E. Tseng and D. Hrovat. *Predictive active steering control for autonomous vehicle systems*. IEEE Trans. on Control System Technology, 15(3), 2007.

[2] P. Falcone, F. Borrelli, J. Asgari, H. E. Tseng and D. Hrovat. *Linear time varying model predictive control and its application to active steering systems: Stability analysis and experimental validation*. International Journal of Robust and Nonlinear Control, 18:862–875, 2008.
[3] R. Rajamani. *Vehicle Dynamics and Control*. Springer, New York, U.S., 2006.
[4] H. B. Pacejka. *Tire and Vehicle Dynamics.* Butterworth-Heinemann, Oxford, UK, 2002.
[5] R. Leenen and H. Schouten. *Virtual Sensors for Advanced Vehicle Stability Control.* 10th International Symposium on Advanced Vehicle Control, 2010.
[6] U. Kiencke and L. Nielsen. *Automotive Control Systems*. Springer, New York, U.S., 2000.